Received: 4 December 2020 | Accepted: 16 March 2021

DOI: 10.1002/term.3194

WILEY

RESEARCH ARTICLE

Using 3D-bioprinting scaffold loaded with adipose-derived stem cells to burns wound healing

Leila Roshangar[1] | Jafar Soleimani Rad[2] | Raziyeh Kheirjou[2] | Ahad Ferdowsi Khosroshahi[3]

[1]Stem Cell Research Center, Tabriz University of Medical Sciences, Tabriz, Iran

[2]Department of Anatomical Sciences, Faculty of Medicine, Tabriz University of Medical Sciences, Tabriz, Iran

[3]Deputy of Education and Research, Imam Reza Hospital, Tabriz University of Medical Sciences, Tabriz, Iran

Correspondence
Ahad Ferdowsi Khosroshahi, Imam Reza Educational and Medical Center, Tabriz University of Medical Sciences, Golgasht St., Tabriz, Iran.
Email: a.ferdosi.kh@gmail.com

Abstract

Three dimensional (3D) printing has recently expanded in popularity and has become an effective approach for tissue engineering. Advances in tissue engineering have increased the effectiveness of cell-based therapies. Indeed, the ultimate goal of such treatment is the development of conditions similar to fetal wound regeneration. In this context, technology of 3D printing also allows researchers to more effectively compose multi-material and cell-laden scaffolds with less effort. In this study, we explored a synthetic gel scaffold derived from 3D bioprinter with or without stem cells to accelerate wound healing and skin defects. Adipose-derived stem cells (ADSCs) were isolated and seeded into 3D bioprinter derived-gel scaffold. Morphological and cell adherence properties of 3D scaffold were assessed by hemotoxylin & eosin (H&E) staining and scanning electron microscopy and cell viability was determined by methylthiazolyldiphenyl-tetrazolium bromide assay. In vivo assessment of the scaffold was done using H&E staining in the full-thickness burn rat model. The experimental groups included; (a) untreated (control), (b) 3D bioprinter derived-gel scaffold (Trial 1), and (c) 3D bioprinter derived-gel scaffold loaded with ADSC (Trial 2). Our results represented 3D bioprinter derived-gel scaffold with or without ADSCs accelerated wound contraction and healing compared to control groups. Epithelization was completed until 21 days after operation in scaffold alone. In scaffold with ADSCs group, epithelization was faster and formed a multi-layered epidermis with the onset of cornification. In conclusion, 3D bioprinter derived-gel scaffold with or without ADSCs has the potential to be used as a wound graft material in skin regenerative medicine.

KEYWORDS
biomaterials, bioprinting, burn, regeneration, skin, tissue

1 | INTRODUCTION

Skin is a vital organ in body with multiple functions including regulation of body temperature, protection of body from environmental agents, and so forth, and damage to this structure can impair its function. Therefore, it is essential to maintain its integrity and repair its damage. Many attempts have been made to repair skin defects in the last decade and allograft and autograft transplantations have been widely used for this purpose. In this regard safety of transplanted tissue, lack of donated samples, and high treatment costs are some of the problems that could be considered (Enoch et al., 2006). Tissue engineering has overcome these problems by substitution of

various tissues and organs using stem cells and biomaterials. Wound healing is a complex process involving several distinct stages and a series of various cells and molecular compounds (Reinke & Sorg, 2012). A number of biomaterials such as cellulose, alginate, collagen, chitin, hyaluronic acid, and so forth have been used to facilitate the wound healing process (Jridi et al., 2015). These biomaterials due to characteristics such as biocompatibility, biodegradability, low toxicity, mechanical stability, maintaining moisture content, and high availability have been effectively used to treat extensive ulcers. They are suitable for the design and construction of scaffolds in tissue engineering. There are many methods to construct scaffolds, including the use of a three-dimensional (3D) printer that create phantom of different parts of the body (Peltola et al., 2008). This technology is used to sediment or implant the living cells into gel media to create 3D functional structures. In fact, the ultimate goal of using this 3D technology is to construct tissue engineering structures to build organs or parts of the body. Many efforts have been done to produce functional and complex 3D bioscaffolds and provide a mimic-biological structure in tissue engineering. Previous articles have explained several types of bioprinting systems with ability to construct 3D cellular or acellular scaffolds. The three most important techniques proposed for construction of a bioprinting system include a laser-induced forward transfer (LIFT), inkjet bioprinting, and robotic dispensing. LIFT is a technique that can sediment cells into a recipient substrate. On the other hand, heterogeneous structures such as skin and bone can be achieved with multiple cells by inkjet bioprinters (Wang et al., 2017). Moreover, based on advances in bioprinting technologies, it is expected that this technology can successfully be used to build a new wound dressing and can maintain a moist wound environment with a minimum of bacterial infection (Mironov et al., 2003; Murphy & Atala, 2014). Therefore, the aim of this study was to examine the possibility of using stem cells with a synthetic gel scaffold derived from extrusion bioprinter to accelerate burn wound healing.

2 | MATERIALS AND METHODS

All the *in vivo* experiments were performed with the approval of the Institutional Animal Ethics Committee of the Tabriz Medical Faculty, Tabriz, Iran (IR.TBZMED.REC.1395.958). The animals were caged individually, feed with food and water ad libitum, in appropriate temperature (23 ± 1°C), with relative humidity 55 ± 5% and were kept under 12 h light/12 h dark cycle.

2.1 | Scalding burn experimental model

It was explained in detail how to create full-thickness burns in rats (Pfurtscheller et al., 2013). Briefly, scalding burns were created with a cylindrical box that has a 2 × 2 cm rectangular hole. All animals were weighed and then preanaesthetized with an acetaminophen 300 mg/kg in drinking water 24 h before operation. After a 6-h fasting, the animals were deep-anesthetized intraperitoneally with 80 mg/kg ketamine 10%, 12 mg/kg xylazine 2%, and 2 mg/kg midazolam. The deep anesthesia was produced after 5–10 min. Thereafter, the back and abdomen of each rat from neck to 2 cm upon rat's tail was carefully shaved with an electric clipper. In the supine position, the animal was fixed onto the cylindrical box from rectangular hole, and a cover was firmly fixed on the rat's abdomen. The cylindrical box was immersed in boiling water from aperture side. After 30 s, the cylindrical box taken out from boiling water and burn's site dried with a pad. In this manner a full-thickness burn wound was created in back area of rat (Figure S1).

2.2 | Fabrication of a mesh structure

A computer-controlled extrusion bioprinter was used for fabrication of a mesh structure and gifted to present study. The applied bioink was the composite of collagen and alginate that arranged layer-by-layer (Zineh et al., 2018) (Figure S1).

2.3 | Characterization of the 3D bioprinter derived-gel scaffold

The morphological and structural characteristics of the 3D scaffold were investigated using an optical microscope (Olympus-BX32, X10 and 40) and a scanning electron microscope (SEM; TESCAN FE-SEM MIRA3).

2.4 | In vitro cell culture and methylthiazolyldiphenyl-tetrazolium bromide assay

The isolation of adipose-derived mesenchymal stem cells (ADSCs) were completely described in other article (Ferdowsi Khosroshahi et al., 2020). The scaffolds were laden with these cells and were cultured in Dulbecco's modified Eagle's medium supplemented 10% fetal bovine serum and 1% antibiotic and incubated at 37°C + 5% CO_2 for 2 days. The proliferation of living cells was determined using the methylthiazolyldiphenyl-tetrazolium bromide (MTT) cell proliferation assay (Cell Proliferation Kit I; Boehringer Mannheim). The assay was based on the cleavage of the yellow tetrazolium salt (MTT) via mitochondrial dehydrogenases in viable cells to produce purple formazan crystals. Cell-loaded structures were incubated in a 0.5 mg/ml MTT solution for 4 h at 37°C. The absorbance at 570 nm was measured using a microplate reader (ELx808™ biotek). Four samples were tested for each incubation period, and each of the tests was performed in triplicate. Finally, the percentage of the cells viability was calculated according to the equation given below.

$$\text{Cell viability percentage} = \frac{(\text{OD sample} - \text{OD blank})}{(\text{OD control} - \text{OD blank})} \times 100.$$

2.5 | Procedures of implantation

Three groups were divided randomly, including (a) untreated (control), (b) 3D bioprinter derived-gel scaffold (Trial 1), and (c) 3D bioprinter derived-gel scaffold loaded with ADSC (Trial 2). Each group included 12 male rats according Table S1. All surgical procedures were performed under strict aseptic condition. Animals were maintained under general anesthesia during surgery with introabdominal injection of ketamine (75 mg/kg body weight) + xylazine (5 mg/kg body weight). A piece of full thickness back skin with size of 2 × 2 cm was burned from each rat and then the necrotic tissue was removed after 24 h. Then a similar in size and form of scaffolds were implanted in wound area and were dressed with transparent dressing until sampling day. Dressings changed every 2–3 days.

2.6 | Scanning electron microscopy

SEM was used to investigate the loading of the cultured cells onto the scaffold. ADSCs were used at the density of 1×10^5 cell onto scaffold. After sterilization using ethylene oxide, cells were seeded onto the scaffolds and incubated at 37°C in a humidified 5% CO_2 atmosphere. For fixation process, the culture media were removed and specimens were washed using phosphate-buffer saline (PBS) and then were incubated in glutaraldehyde 10% (Sigma-Aldrich) for 90 min at room temperature. Fixative solution was then removed and scaffolds were washed with PBS. Dehydration was carried out using a series of increasing concentration of ethanol (30%, 50%, 70%, 80%, 90%, and 100%), 10 min per each concentration. Sample were finally dried, covered by 1 nm thickness golden layer, and investigated using an SEM machine.

2.7 | Postoperative wound assessment

All the wounds were dressed with tetracycline impregnated sterile gauze and covered with a transparent dressing. This dressing prevents the adhesion of the implanted element to the wound site and can be easily separated when changing the dressing. Digital photographs were captured at each time point for macroscopic assessment. To measure the wound surface and wound healing rate, images were analyzed by Image J 1.43c software (imagej.net) in mm^2. At each time point, the animals were sacrificed in a standard manner, and sampling was done from the wound site. Specimens were prepared with histopathology and IHC methods. A blinded pathologist surveyed the microscopic samples in terms of infiltration of inflammatory cells, re-epithelialization, collagen synthesis and rearrangements, and rate of revascularization. All sections were compared under a light microscope, and these factors were digitally quantified on the surface unit of the tissue slide using Grid cell counter v 0.9.9 software.

2.8 | Evaluation of histology and IHC

For this purpose, fresh specimens were harvested at 21 days after implantation and were fixed in 10% neutral buffered formalin (Sigma-Aldrich), dehydrated in increasing concentrations of ethanol (70%, 90%, and 100%) for 30 min and immersed twice in xylene for 30 min followed by a 30 min immersion in liquid paraffin for impregnation. The paraffin-embedded specimens were sectioned at 5-lm thickness and were stained by hematoxylin and eosin (H&E) (Leica), Masson trichrome (Sigma-Aldrich), and immunohistochemistry (IHC). IHC staining was done to investigate pan-cytokeratin AE1/AE3 (NBP2-29,429) and P63 (ab124762) as epithelial markers and CD34 (AF4117-SP) as a vascularization marker.

2.9 | Statistical analysis

Statistics were performed with the SPSS statistics program (windows version 16). All analytical data were expressed as mean ± standard deviation from three independent experiments. Statistical analyses were conducted using one-way analysis of variance and unpaired *t* test; $p < 0.05$ was considered statistically significant.

3 | RESULTS

3.1 | Histological and SEM analysis

Images of H&E staining by optical microscope and scanning electron micrographs of ultrastructural properties of scaffold were shown the suitable pores in different sizes for 3D bioprinter matrix that have capacity to the stem cells (Figure 1 a,b).

3.2 | Cell viability assessment

MTT analysis showed that there was no significant difference between the optical density (OD) values measured in 24 h between 3D bioprinter derived-gel scaffold groups compared to control groups. But a significant increase of OD values was detected between scaffold groups compared to control after 48 h and also between 24 and 48 h of treated groups ($p < 0.0001$). MTT test results showed that 3D bioprinter derived-gel scaffold was not only toxic but also promoted the percent of the viability of cultured cells (72.21 ± 9% in scaffold groups vs. 47.02 ± 8.34% in control groups). Although this difference is not significant ($p = 0.87$) (Figure 1 c,d).

3.3 | 3D bioprinter derived-gel scaffold enhanced the burn wounds healing

Although *in vitro* studies shown that the 3D bioprinter derived-gel scaffold increases cell adhesion to the scaffold and proliferates it.

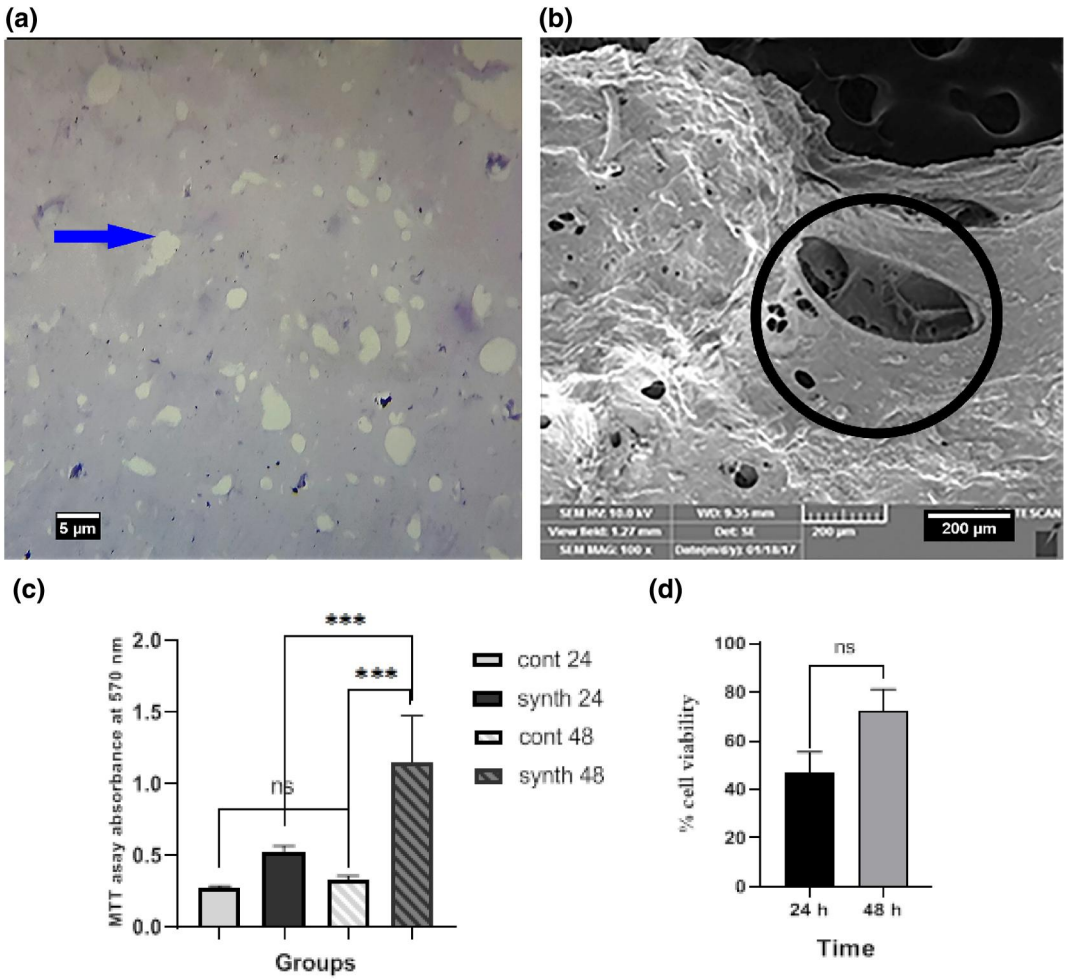

FIGURE 1 H&E & scanning electron micrographs (SEM) of 3D bioprinter derived-gel scaffold (a) and (b), respectively. Arrow show pores in 3D bioprinter derived-gel scaffold that cells-laden were shown in pores of this scaffold in SEM graph (circle mark). (c) MTT assay absorbance and percentage of cell viability of ADSC cells cultured on scaffolds made of 3D bioprinter. (d) Cell viability percent of ADSCs cultured on two consecutive times (24–48 h). 3D, three-dimensional; ADSC, adipose-derived stem cell; H&E, hemotoxylin & eosin; MTT, methylthiazolyldiphenyl-tetrazolium bromide. $^{*}p < 0.0001$

Burn wound healing also was studied in this study by implantation of 3D bioprinter derived-gel with or without ADSCs. According to the studies, after implantation for 21 days, both 3D bioprinter derived-gel with or without ADSCs significantly increased the burn wound healing and the closure rates were 16 ± 2 and 56 ± 2 mm^2, respectively, while that in the control was 223 ± 10 mm^2 (Table S1 and Figure S2). The regeneration of epidermis and dermis layers starts with cell migration of wound edges into the wound, and the histological appearance of the wound tissue was completed on Day 21. H&E staining and counting of leukocytes (lymphocytes and neutrophils), new blood vessels and fibroblasts were evaluated at three time point after scaffold implantation and was shown in Figure S2 and S3 and Table S2 (Konop et al., 2020). These results revealed that new epidermal and dermal tissues were regenerated only in defects implanted with scaffolds. At 21 days, a new thickness epidermal layer and granulation tissue were observed in Trial 2, whereas partial epithelization was only observed in Trial 1, and no epithelization was observed in untreated group. In addition, in control group, partial inflammation was absent and underlying epidermis represented fibrous tissue and neovascularization (Figure 2e). Complete epithelialization and mild fibrous tissue were observed in trial 2 group and neovascularization looks like normal skin. Collagen fibers were dense, thick, and better arranged at these groups (Figure 2f). The histological changes in Trial 2 and Trial 1 were similar together, with this difference that fibrous tissue was absent and collagen fibers were arranged in the best possible condition.

3.4 | Histochemistry analysis of in vivo skin burn wound

In the microscopic observations of the trichrome staining, a different connective tissue density was observed between different groups based on the intensity of blue color, with the results being shown in Figure 3. There were absolutely dense collagen fibers and connective tissue (clear blue color) in the trial and control groups. Although the 3D

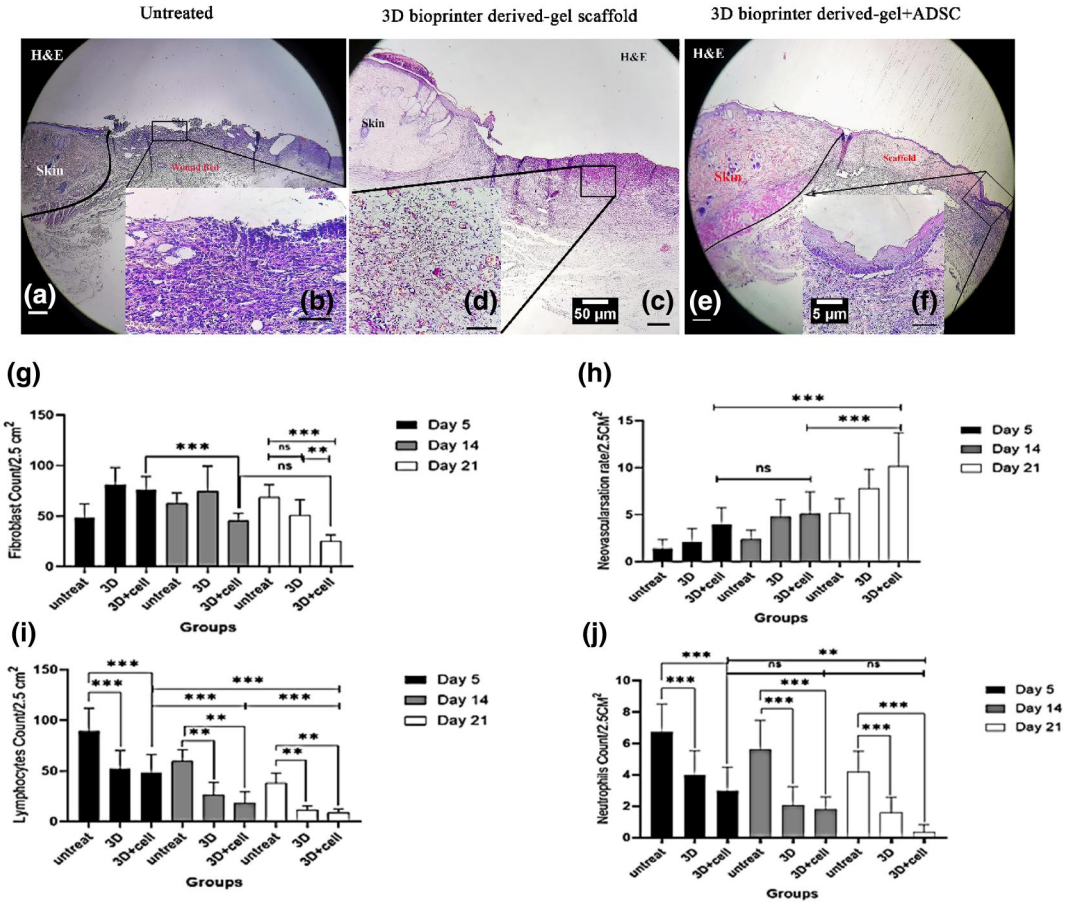

FIGURE 2 (a–f) Histological analysis of *in vivo* skin burn wound healing 21 days after implantation. Arrows show epidermal layer in treatment groups compare to control groups. Cycle mark shows vascular formation scaffold site. Scale bar = 50 μm for full size images and 5 μm for insets. (g–j) Diagram of mean of number of cells counted in different groups at three time point. The number of fibroblasts in the trial and control groups increased from Day 5 to 14 and gradually decreased to Day 21, indicating better deposition of collagen in these groups. The number of new blood vessels, especially in trial groups, increased from Day 5 to 21. The number of lymphocytes in trial groups decreased from Day 5 to 21. At Day 5, the number of lymphocytes in the implantation site in control groups showed a significant increase compared to sham groups. Comparison of this group with trial groups at this time showed a significant decrease in these cells and the inflammation subsides at the wound site; and it is possibly indicates the immunomodulatory role of adipose-derived mesenchymal cells. Finally, the number of neutrophils in trial groups decreased from Day 5 to 21

scaffold with or without ADSCs can clearly cover the surface of the burn wound on Day 5 postoperation, only in trial groups, a suitable integration is observed with the wound margins at this time, and this integration became complete with skin collagen fiber after Day 21 (Figure 3). This integration guarantees regular structure and arrangement of the reproduced collagen fiber. On the other hand, the collagen fiber in the control groups was observed as irregular beside numerous blood vessels. In untreated group, lack of deposition and organization of collagen fibers was observed in the necrosis tissue formed at Day 5. As well as lack of integration with the wound margins along with an accumulation of blood cells in site of the wound was observed in this group on Day 21. In trial groups, the deposition and distribution of collagen fibers were been better and more regular compared to control groups, and in some regions, some elements of skin appendages were also formed, especially in Trial 2 groups.

The granulation tissue in the trial groups was well formed in the wound matrix on Day 14, suggesting development of good neovascularization at the site of wound after this time. In a comparison of the trial groups with control groups, a significant rise was observed in the thickness of the granulation tissue. Presence of this suitable granulation tissue in the wound matrix suggests preparation of the wound to receive the implant in the trial groups and integration with the wound margins and development of a suitable cover for the site of burn.

4 | IHC ANALYSIS OF IN VIVO SKIN BURN WOUND

4.1 | Pan-cytokeratin AE1/AE3 analysis

The expression of pan-cytokeratin AE1/AE3 on Day 21 was seen in the trial groups with a dark brown staining in the epithelial layer in

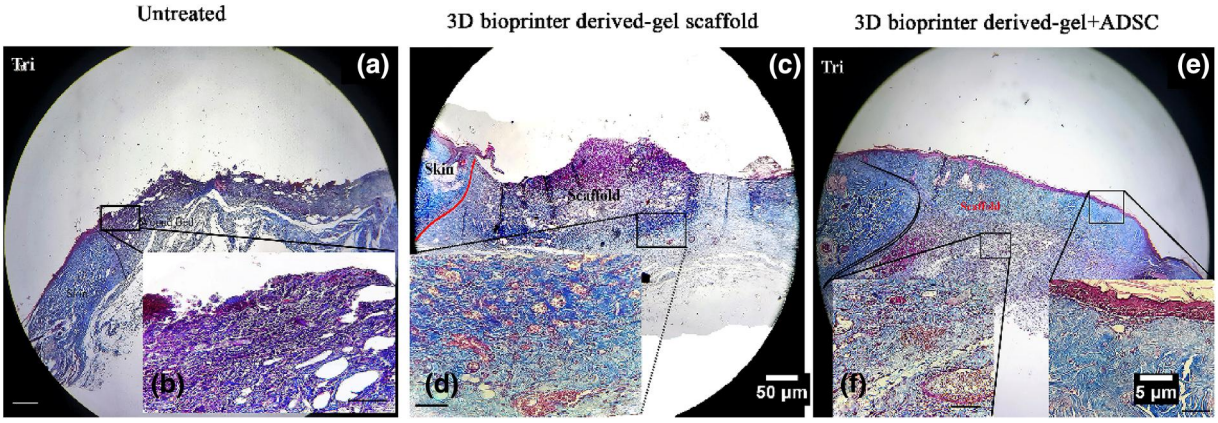

FIGURE 3 Trichrome staining of *in vivo* skin burn wound healing 21 days after implantation. In untreated group (a,b), lack of deposition and organization of collagen fibers was observed and accumulation of blood cells shifted to the site of wound. The collagen fiber in the control groups (c,d) was observed as irregular beside numerous blood vessels. In trial groups (e,f), the deposition and distribution of collagen fibers were been better and more regular, and in some regions, some elements of skin appendages were also formed. Scale bar = 50 μm for full size images and 5 μm for insets

comparison with control groups, which were not formed any stratified layer (Figure 4). This cytokeratin can be tracked and observed in the epidermis layer as dark brown staining in comparison to the light brown color of the dermis layer. In addition, this marker is also visible in the cells of other skin appendages in case of formation.

4.2 | P63^{+} cells counting

The population of P63+ epithelial cells in 1 × 1 μm microscopic field of epithelium was counted under ×10 magnifications. Concerning the population of these cells, the difference between the natural epithelium of the skin and control as well as trial groups has been shown in Figure 5. In comparison to normal skin ($N = 15.5 \pm 2.25$), P63+ cell population in Trial 2 groups was 14.52 ± 3.75 which does not show any significant change ($p = 0.15$). This suggests that the 3D scaffold in the presence of ADSCs has developed neoepithelialization at the site of burn wound. However, in Trial 1 and control groups, no cell population with P63+ surface marker was observed in the center of wound site.

4.3 | CD34 marker analysis

In this study, the newly formed blood vessels containing blood cells that have absorbed brown color were considered as the criterion for neovascularization. Accordingly, based on Figure 6, in control groups, the blood vessels were formed as pseudovessel, in Trial 1 groups as mild, and in the Trial 2 groups as moderate to severe. Gradually, these vessels penetrated from the wound matrix to the bottom of epithelium. Also, the number of blood cells inside the vessels was increased.

5 | DISCUSSION

The main purpose of this study was to investigate the efficacy of the 3D bioprinter derived-gel scaffold with and without ADSCs in full-thickness burn wound healing in rat model. The results of this study showed that the scaffold without or with ADSCs improve burn wound compared to control group. In various studies were shown that ADSCs have epithelial potential (Na et al., 2017). In gross observation and histological evaluation, the structure of all bioprinted scaffold was homogenous, with a regularly space. Morphological characterization of 3D bioprinter scaffold had been reported by Berg et al. (2018), as well as Naghieh et al. (2019), which is a useful manner to assess changes in the scaffold's microstructure. Based on our results of the SEM study, during the 24-h culture period, the cells had good adhesion to the scaffold, and the existence of cellular filopodia indicated an effective communication of the cells with each other as well as the relationship of the cells with scaffold. MTT assay results in this study indicated that although the percentage of viability of ADSCs was not significant from 24 to 48 h, however, an increase was visible. It shows produced scaffold in this study was not toxic and could be led to the proliferation of the cells. The second part of the present study was the in vivo study that evaluates the efficiency of 3D bioprinter derived-gel scaffold on rat skin burn defects, with or without ADSCs.

Cui et al. (2012) reported a 3D structure containing stem cells, smooth muscle cells, and endothelial cells using a thermal inkjet printer. The results of their experiments showed that these printed cells in in vitro can survive, proliferate, and keep cellular function in this 3D structure (Cui et al., 2012). More importantly, stem cells and endothelial cells were able to differentiate into bone and blood vessels 6 weeks later after transplanting to mice (Wang et al., 2016). In numerous studies, collagen type I was used as a hydrogel scaffold to seed cells in the printing process and extracellular matrix

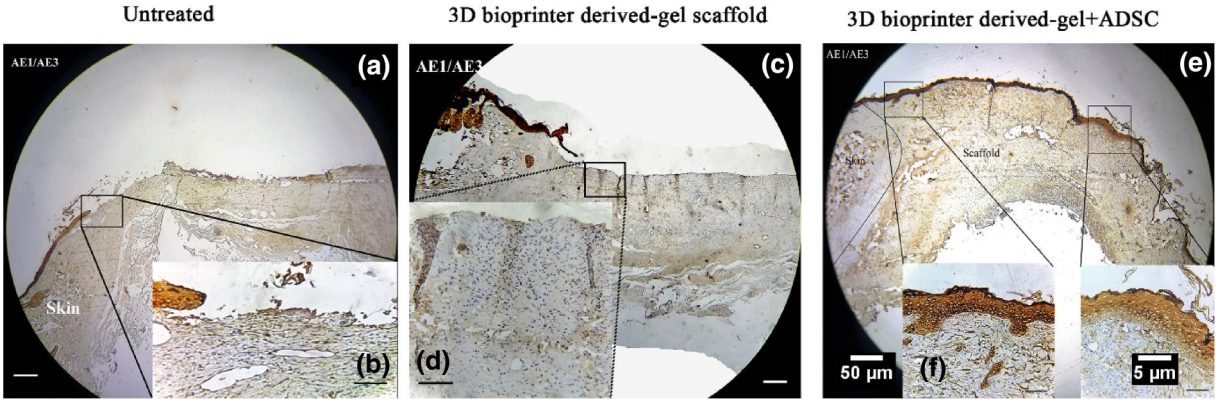

FIGURE 4 Pan-cytokeratin AE1/AE3 analysis of *in vivo* skin burn wound healing 21 days after implantation. The expression of these markers were seen in the trial groups (e,f) with a dark brown staining in the epithelial layer in comparison with control (c,d) and untreated (a,b) groups. Scale bar = 50 µm for full size images and 5 µm for insets

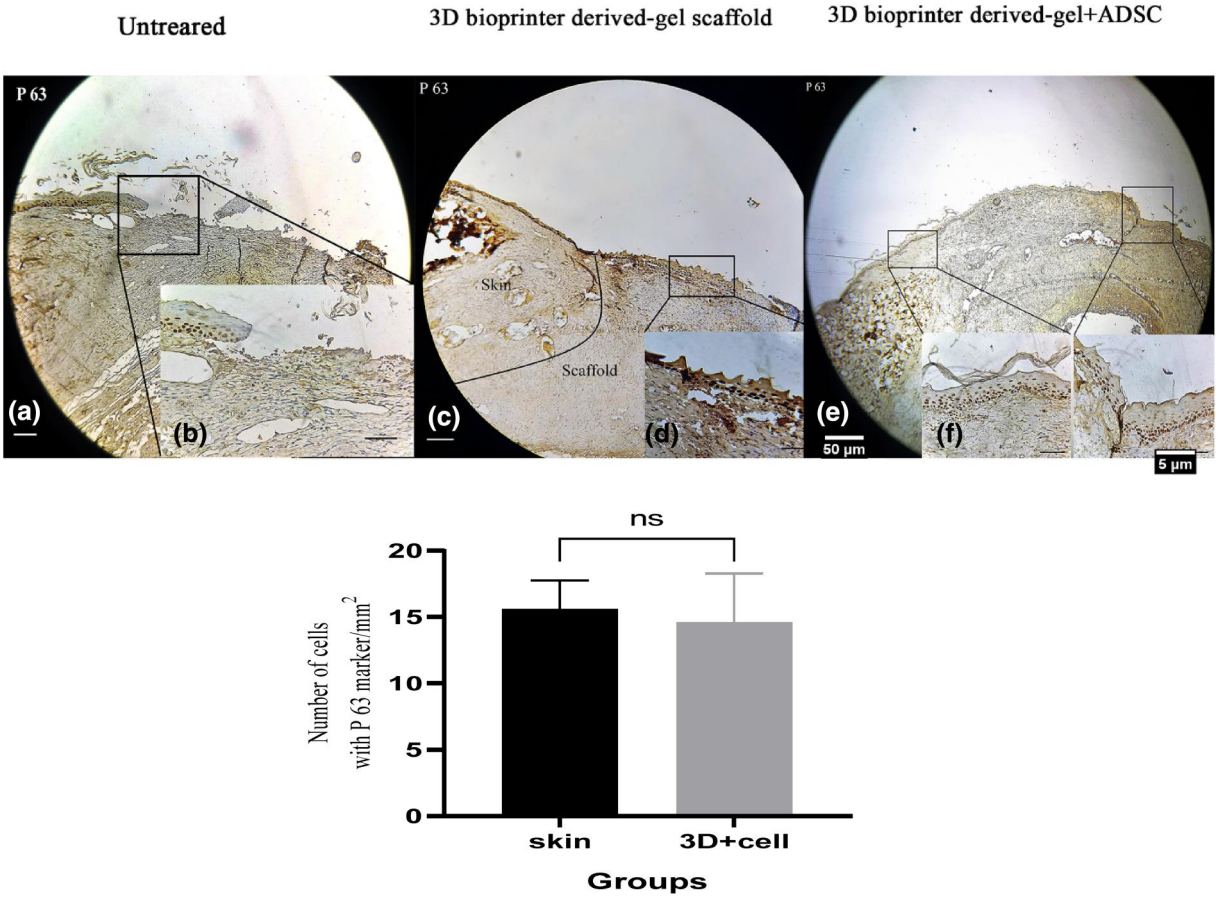

FIGURE 5 P63^{+} marker analysis of *in vivo* skin burn wound healing 21 days after implantation. In trial groups (e,f), the 3D scaffold in the presence of ADSCs has developed neoepithelialization at the site of burn wound. However, in the control (c,d) and untreated (a,b) groups, no cell population with P63+ surface marker was observed. Scale bar = 50 µm for full size images and 5 µm for insets. 3D, three-dimensional; ADSC, adipose-derived stem cell ($p = 0.15$)

conditions had created almost like normal skin. These studies have been carried out to optimize bioprinter parameters and increase cell viability, and also optimize the density of epidermal and dermal cells to imitate the physiological characteristics of the human skin (V. Lee et al., 2013; W. Lee et al., 2009). Another study showed that 20 layers of fibroblasts and 20 layers of keratinocytes, which were placed in collagens of Matriderm® (a decellularized scaffold) by a laser bioprinter, were suitable for the production of a simple 3D skin with a structure similar to dermis and epidermis (Koch et al., 2012). The results indicate that the printed cells survived well and

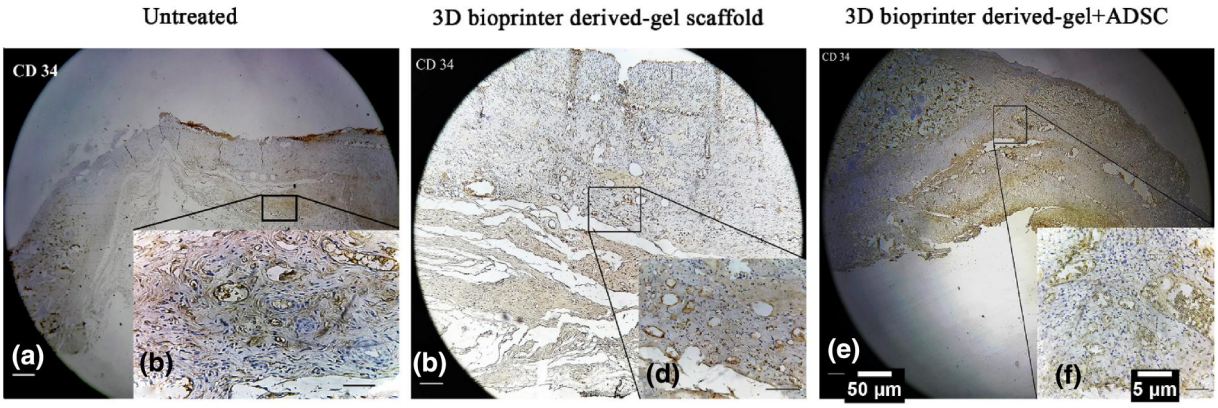

FIGURE 6 CD34 marker analysis of *in vivo* skin burn wound healing 21 days after implantation. In untreated groups (a,b), the blood vessels were formed as pseudovessel, in the control groups (c,d) as mild, and in the trial groups (e,f) as moderate to severe. Scale bar = 50 μm for full size images and 5 μm for insets

reangiogenesis was observed in the skin structure under in vivo conditions. In other study similar double-layer structures were made in vitro and transplanted into dorsal part of the nude mice (Michael et al., 2013). They found that printed keratinocytes form a multilayered epidermis with the onset of cornification, and printed fibroblasts could produce collagen and extracellular matrix. In addition, some blood vessels were seen in the wound bed 11 days after transplantation. In recent years, the integration of bioprinting technologies with stem cell research is an emerging field. Stem cells such as bone marrow stem cells, embryonic stem cells, and ADSCs have been reported to act as bioink bioprinter substrate for skin regeneration (Gruene et al., 2010; Tricomi et al., 2016; Xu et al., 2011). In this study the histological data from Trial 2 groups showed that wound healing and contraction occurred until 21 days. Both trial groups accelerated wound contraction and healing compared to control groups. Although wound area was completely repaired in the Trial 2 groups at 21 days without any scar formation.

Since the aim of this study in the in vivo section was the examination of the performance of 3D scaffold loaded with ADSCs in repairing and regenerating third-degree burn wounds, this work was examined with histological and IHC techniques. In in vivo part of the study, the full-thickness burn wound was created in the rats' back region and the results indicated that the regeneration of wound was better in the trial groups compared to the control groups. Analysis of macroscopic data of the Trial 2 groups indicated that repair and closure of wound occurred completely during 21 days in these groups. Moreover, based on microscopic images, in the Trial 2 groups by creating a continuous epidermal layer at a considerable distance from the wound margins and as well as observation of growth of sebaceous glands, it can be introduced that repair has occurred and wound contraction has not happened. Recently, various studies have shown that mesenchymal cells participate in regeneration of hair follicles and sebaceous glands (Chen et al., 2012; Hocking & Gibran, 2010; Li et al., 2006). Furthermore, decrease the extent of infiltration of inflammatory cells in both trial groups compared to the control groups on Day 5, possibly show the immunomodulatory role of ADSCs (Puissant et al., 2005). On the fifth day, in all of the groups, neutrophils and lymphocytes were present. In the bed of 3D bioprinter derived-gel scaffold, especially in Trial 2 groups the number of these cells were decreased after that time point. Although the presence of the inflammatory cells is more preferable during the healing process, the continuing of this process leads to produce scar tissue. In contrast, in control wounds, neutrophils predominated at this time point with lymphocytes (Konop et al., 2020). On the 21st day, epithelialization expanded greater and faster in the Trial 2 groups compared to the control and Trial 1 groups, and had covered the surface of wound, which can be due to participation of mesenchymal cells and their ability in control of inflammation. It has been shown that inflammation plays a significant role in the repair and regeneration of wounds especially in lack of formation of scars (Xiao et al., 2014). Furthermore, these cells affect the modification of the immune system reaction and differentiation into different skin cells including fibroblasts and keratinocytes and eventually improving the course of wound regeneration (Parmaksiz et al., 2017).

Analysis of the data obtained from IHC for AE1/AE2 epithelial marker at the site of graft in Trial 2 groups compared to Trial 1 groups indicated a structured epidermis layer (horny layer on top of the basal layer). Furthermore, observation of a larger number of cells with p63 marker in the basal layer of epidermis and their gradual reduction in the basal layer similar to normal skin confirms progressive differentiation of ADSCs to keratinocytes and reformation of epithelium across the implant scaffold. Epithelialization is essential for repairing burn wounds, which confers protection against infection and preserves the balance of fluids (Tiwari, 2012).

The integration in the host tissue and neovascularization is necessary for wound repair. This occurs first through penetration of inflammatory cells from wound margin to the scaffold and following matrix regeneration and the final neovascularization. The rate of repair of the wound is possibly associated with the extent of diffusion of nutrients inside the scaffold. In this study, the results of H&E and trichrome staining, and counts of vessels indicated that formation of this tissue and blood vessels summoned up to this site essential for

transferring nutrients and oxygen has well occurred on Day 14 in trial groups. Furthermore, based on trichrome staining and counting of fibroblasts, the density of collagen fibers and the number of these cells in the Trial 2 groups have decreased (low blue staining) in comparison to Trial 1 and control groups. Analysis of CD34+ cells in IHC indicates the existence of blood vessel cells in the matrix of the implanted scaffold in the wound bed. Although some of them are blood cells, CD34 is also known as the marker of the endothelial cells of the blood vessels. Some of these cells are probably phagocytic and degrading cells, which constitute part of the course of wound healing. A previous study using ADM observed recellularization during the first 7 days which accompany with increase myofibroblasts and positive CD31 endothelial cells (Wong et al., 2008). The positivity of CD34 was greater in the Trial 2 groups compared to the control or Trial 1 groups on Day 21, which grew from the depth to the surface of wound at this time point. Previous studies have shown that Integra® was revascularized at Day 14 (Shaterian et al., 2009), which are similar to our findings.

In the present study, we did not mark and track the migration and integration of ADSCs in the regenerated skin. Although the results of employing the cells were far more effective than cell-free treatments, an increase in cells can still be useful to present structural support for skin regeneration. Note that the stimulation of the cells printed by the carrier material (collagen gel/chitosan) might be limited. Collagen and chitosan are materials that highly cell adhesive, and may inhibit the mobility of cells; they potentially limit the full potential of printed cells.

6 | CONCLUSION

Due to the self-renewal characteristics of stem cells and the differentiation potential into different cell lines; and considering the survival rate of printed cells is high and it has been reported that the survival rate of stem cells before and after using the 3D bioprinter is 97% and 94%, respectively (Han et al., 2012), which allows to effective wound healing. Therefore, the ADSCs seeded in 3D bioprintering scaffold can provide a suitable environment for cells regeneration and wound healing.

ACKNOWLEDGMENT

The authors would like to thank the colleagues of Tissues Engineering Lab of Medicine Faculty of Tabriz University of Medical Sciences for the support provided for this research.

CONFLICT OF INTERESTS

The authors declare that they have no known competing financial interests or personal relationships that could have appeared to influence the work reported in this paper.

DATA AVAILABILITY STATEMENT

Our data are available to share.

ORCID

Ahad Ferdowsi Khosroshahi https://orcid.org/0000-0002-8679-3755

REFERENCES

Berg, J., Hiller, T., Kissner, M. S., Qazi, T. H., Duda, G. N., Hocke, A. C., Hippenstiel, S., Elomaa, L., Weinhart, M., Kurreck, C., & Fahrenson, C. (2018). Optimization of cell-laden bioinks for 3D bioprinting and efficient infection with influenza A virus. *Scientific Reports*, *8*(1), 13877.

Chen, S.-G., Tzeng, Y.-S., & Wang, C.-H. (2012). Treatment of severe burn with DermACELL®, an acellular dermal matrix. *International Journal of Burns and Trauma*, *2*(2), 105.

Cui, X., Boland, T., D'Lima, D., & Lotz, M. K. (2012). Thermal inkjet printing in tissue engineering and regenerative medicine. *Recent Patents on Drug Delivery & Formulation*, *6*(2), 149–155.

Enoch, S., Grey, J. E., & Harding, K. G. (2006). Recent advances and emerging treatments. *BMJ*, *332*(7547), 962–965.

Ferdowsi Khosroshahi, A., Soleimani Rad, J., Kheirjou, R., Roshangar, B., Rashtbar, M., Salehi, R., Ranjkesh, M. R., & Roshangar, L. (2020). Adipose tissue-derived stem cells upon decellularized ovine small intestine submucosa for tissue regeneration: An optimization and comparison method. *Journal of Cellular Physiology*, *235*(2), 1556–1567.

Gruene, M., Deiwick, A., Koch, L., Schlie, S., Unger, C., Hofmann, N., Bernemann, I., Glasmacher, B., & Chichkov, B. (2010). Laser printing of stem cells for biofabrication of scaffold-free autologous grafts. *Tissue Engineering C Methods*, *17*(1), 79–87.

Han, Y., Tao, R., Sun, T., Chai, J., Xu, G., & Liu, J. (2012). Advances and opportunities for stem cell research in skin tissue engineering. *European Review for Medical and Pharmacological Sciences*, *16*(13), 1873–1877.

Hocking, A. M., & Gibran, N. S. (2010). Mesenchymal stem cells: Paracrine signaling and differentiation during cutaneous wound repair. *Experimental Cell Research*, *316*(14), 2213–2219.

Jridi, M., Bardaa, S., Moalla, D., Rebaii, T., Souissi, N., Sahnoun, Z., & Nasri, M. (2015). Microstructure, rheological and wound healing properties of collagen-based gel from cuttlefish skin. *International Journal of Biological Macromolecules*, *77*, 369–374.

Koch, L., Deiwick, A., Schlie, S., Michael, S., Gruene, M., Coger, V., Zychlinski, D., Schambach, A., Reimers, K., Vogt, P. M., & Chichkov, B. (2012). Skin tissue generation by laser cell printing. *Biotechnology and Bioengineering*, *109*(7), 1855–1863.

Konop, M., Czuwara, J., Kłodzińska, E., Laskowska, A. K., Sulejczak, D., Damps, T., Zielenkiewicz, U., Brzozowska, I., Sureda, A., Kowalkowski, T., Schwartz, R. A., & Rudnicka, L. (2020). Evaluation of keratin biomaterial containing silver nanoparticles as a potential wound dressing in full-thickness skin wound model in diabetic mice. *Journal of Tissue Engineering and Regenerative Medicine 14*(2), 334–346.

Lee, V., Singh, G., Trasatti, J. P., Bjornsson, C., Xu, X., Tran, T. N., Yoo, S.-S., Dai, G., & Karande, P. (2013). Design and fabrication of human skin by three-dimensional bioprinting. *Tissue Engineering Part C Methods*, *20*(6), 473–484.

Lee, W., Debasitis, J. C., Lee, V. K., Lee, J.-H., Fischer, K., Edminster, K., Park, J.-K., & Yoo, S.-S. (2009). Multi-layered culture of human skin fibroblasts and keratinocytes through three-dimensional freeform fabrication. *Biomaterials*, *30*(8), 1587–1595.

Li, H., Fu, X., Ouyang, Y., Cai, C., Wang, J., & Sun, T. (2006). Adult bone-marrow-derived mesenchymal stem cells contribute to wound healing of skin appendages. *Cell and Tissue Research*, *326*(3), 725–736.

Michael, S., Sorg, H., Peck, C.-T., Koch, L., Deiwick, A., Chichkov, B., Vogt, P. M., & Reimers, K. (2013). Tissue engineered skin substitutes

created by laser-assisted bioprinting form skin-like structures in the dorsal skin fold chamber in mice. *PLoS One*, *8*(3), e57741.

Mironov, V., Boland, T., Trusk, T., Forgacs, G., & Markwald, R. R. (2003). Organ printing: Computer-aided jet-based 3D tissue engineering. *Trends in Biotechnology*, *21*(4), 157–161.

Murphy, S. V., & Atala, A. (2014). 3D bioprinting of tissues and organs. *Nature Biotechnology*, *32*(8), 773.

Na, Y. K., Ban, J.-J., Lee, M., Im, W., & Kim, M. (2017). Wound healing potential of adipose tissue stem cell extract. *Biochemical and Biophysical Research Communications*, *485*(1), 30–34.

Naghieh, S., Sarker, M. D., Abelseth, E., & Chen, X. (2019). Indirect 3D bioprinting and characterization of alginate scaffolds for potential nerve tissue engineering applications. *Journal of the Mechanical Behavior of Biomedical Materials*, *93*, 183–193.

Parmaksiz, M., Elcin, A. E., & Elcin, Y. M. (2017). Decellularization of bovine small intestinal submucosa and its use for the healing of a critical-sized full-thickness skin defect, alone and in combination with stem cells, in a small rodent model. *Journal of Tissue Engineering and Regenerative Medicine*, *11*(6), 1754–1765.

Peltola, S. M., Melchels, F. P. W., Grijpma, D. W., & Kellomäki, M. (2008). A review of rapid prototyping techniques for tissue engineering purposes. *Annals of Medicine*, *40*(4), 268–280. https://doi.org/10.1080/07853890701881788

Pfurtscheller, K., Petnehazy, T., Goessler, W., Wiederstein-Grasser, I., Bubalo, V., & Trop, M. (2013). Innovative scald burn model and long-term dressing protector for studies in rats. *Journal of Trauma and Acute Care Surgery*, *74*(3), 932–935.

Puissant, B., Barreau, C., Bourin, P., Clavel, C., Corre, J., Bousquet, C., Taureau, C., Cousin, B., Abbal, M., Laharrague, P., Penicaud, L., Casteilla, L., & Blancher, A. (2005). Immunomodulatory effect of human adipose tissue-derived adult stem cells: Comparison with bone marrow mesenchymal stem cells. *British Journal of Haematology*, *129*(1), 118–129.

Reinke, J. M., & Sorg, H. (2012). Wound repair and regeneration. *European Surgical Research*, *49*(1), 35–43.

Shaterian, A., Borboa, A., Sawada, R., Costantini, T., Potenza, B., Coimbra, R., Baird, A., & Eliceiri, B. P. (2009). Real-time analysis of the kinetics of angiogenesis and vascular permeability in an animal model of wound healing. *Burns*, *35*(6), 811–817.

Tiwari, V. K. (2012). Burn wound: How it differs from other wounds? *Indian Journal of Plastic Surgery*, *45*(2), 364.

Tricomi, B. J., Dias, A. D., & Corr, D. T. (2016). Stem cell bioprinting for applications in regenerative medicine. *Annals of the New York Academy of Sciences*, *1383*(1), 115–124.

Wang, K., Ho, C.-C., Zhang, C., & Wang, B. (2017). A review on the 3D printing of functional structures for medical phantoms and regenerated tissue and organ applications. *Engineering*, *3*(5), 653–662.

Wang, X., Ao, Q., Tian, X., Fan, J., Wei, Y., Hou, W., Tong, H., & Bai, S. (2016). 3D bioprinting technologies for hard tissue and organ engineering. *Materials*, *9*(10), 802.

Wong, A. K., Schonmeyer, B. H., Singh, P., Carlson, D. L., Li, S., & Mehrara, B. J. (2008). Histologic analysis of angiogenesis and lymphangiogenesis in acellular human dermis. *Plastic and Reconstructive Surgery*, *121*(4), 1144–1152.

Xiao, M., Li, L., Li, C., Zhang, P., Hu, Q., Ma, L., & Zhang, H. (2014). Role of autophagy and apoptosis in wound tissue of deep second-degree burn in rats. *Academic Emergency Medicine*, *21*(4), 383–391.

Xu, F., Sridharan, B., Wang, S., Gurkan, U. A., Syverud, B., & Demirci, U. (2011). Embryonic stem cell bioprinting for uniform and controlled size embryoid body formation. *Biomicrofluidics*, *5*(2), 022207.

Zineh, B. R., Shabgard, M. R., & Roshangar, L. (2018). Mechanical and biological performance of printed alginate/methylcellulose/halloysite nanotube/polyvinylidene fluoride bio-scaffolds. *Materials Science and Engineering C*, *92*, 779–789.

SUPPORTING INFORMATION

Additional supporting information may be found online in the Supporting Information section at the end of this article.

How to cite this article: Roshangar L, Rad JS, Kheirjou R, Khosroshahi AF. Using 3D-bioprinting scaffold loaded with adipose-derived stem cells to burns wound healing. *J Tissue Eng Regen Med*. 2021;1–10. https://doi.org/10.1002/term.3194